Environmental Research 272 (2025) 121159

Contents lists available at ScienceDirect

Environmental Research

journal homepage: www.elsevier.com/locate/envres

Impacts of repeated photochemical and microbial processes: Selectively shaping of the dissolved organic matter pool

Qi Chen [a,b,c,*], Christian Lønborg [d], Jiaxin Chen [a,b], Stephen J. Giovannoni [c], Chen He [e], Kunshan Gao [a], Quan Shi [e], Nianzhi Jiao [a,b], Qiang Zheng [a,b,**]

[a] State Key Laboratory for Marine Environmental Science, College of Ocean and Earth Sciences, Xiamen University, Xiamen, China
[b] Fujian Key Laboratory of Marine Carbon Sequestration, Xiamen University, Xiamen, China
[c] Department of Microbiology, Oregon State University, Corvallis, OR, USA
[d] Section for Marine Diversity and Experimental Ecology, Department of Ecoscience, Aarhus University, Roskilde, Denmark
[e] State Key Laboratory of Heavy Oil Processing, China University of Petroleum, Beijing, China

ARTICLE INFO

Keywords:
Dissolved organic matter
Photochemical degradation
Microbial degradation
Chemical composition
Microbial community composition

ABSTRACT

Abiotic photochemistry and microbial degradation are the two main removal processes of marine dissolved organic matter (DOM). However, the combined and repeated effects of irradiation and biodegradation on DOM remains poorly resolved due to their complex interactions. To disentangle the effects of abiotic photochemistry from photobiology, we alternately exposed coastal DOM to repeated exposures to simulated solar radiation and then to microbial communities in darkness. Our results demonstrated selective impacts on the DOM pool by photochemical and microbial degradation. Photodegradation resulted in the loss of fluorescent (both protein- and humic-like), the enrichment of aliphatic and nitrogen-containing compounds, and an increase in microbial diversity. However, biodegradation drove changes in key molecules (significantly altered) and enhanced the contribution of alicyclic compounds and aromatic compounds containing carboxyl/ester functional groups. Network analysis implicated the irradiation adapted (i.e., *Methylophagaceae*) microbes in DOM transformations involving the gain and loss of methyl groups, while the non-irradiation adapted (i.e., *Alteromonadaceae*) microbes appeared to alter DOM composition by the gain and loss of oxygen atoms. Our findings distinguish the selective contributions of irradiation and biodegradation processes and point to the complex interactions between photochemical and biological processes that jointly shape the DOM pool.

1. Introduction

Dissolved organic matter (DOM) represents the largest reduced carbon pool in the ocean and serves as a cornerstone of all major biogeochemical cycles (Hansell et al., 2009; Jiao et al., 2010). In the open ocean, DOM is mainly produced by plankton, while in coastal waters, it is supplemented by many additional sources, predominantly from riverine input (Harrison et al., 2005; Moran et al., 2022). DOM undergoes transformation and removals through photochemical and microbial processes, or through sorption to particles followed by sedimentation (Carlson and Hansell, 2015; Wen et al., 2022). These processes lead to both quantitative and qualitative changes in the DOM pool (Carlson and Hansell, 2015; Jiao et al., 2014; Siegel et al., 2002). Photochemical and microbial degradation are considered to be the primary drivers of DOM breakdown, but their relative importance depends on the chemical compositions of DOM and microbial community composition, as well as spatial and temporal factors (Seidel et al., 2015; Song et al., 2022).

Photochemical degradation of DOM is initiated by absorption of ultraviolet (UV) light by its coloured or chromophoric fraction (CDOM) (Mopper et al., 2015). This absorption triggers a cascade of reactions, leading to the completely transformation of DOM into inorganic carbon or the production of new compounds that are often less humified with lower molecular weight (Holt et al., 2021; Li et al., 2020). Microbes comprise the majority of living organism in the ocean and dominate biologically mediated DOM degradation (Azam et al., 1983; Bar-On and Milo, 2019). Their diverse metabolic capacities and strategies enable microbes to constantly transform organic compounds, such as

* Corresponding author. State Key Laboratory for Marine Environmental Science, College of Ocean and Earth Sciences, Xiamen University, Xiamen, China.
** Corresponding author. State Key Laboratory for Marine Environmental Science, College of Ocean and Earth Sciences, Xiamen University, Xiamen, China.
E-mail addresses: chenq7@oregonstate.edu (Q. Chen), zhengqiang@xmu.edu.cn (Q. Zheng).

https://doi.org/10.1016/j.envres.2025.121159
Received 16 January 2025; Received in revised form 9 February 2025; Accepted 17 February 2025
Available online 18 February 2025

converting labile forms to recalcitrant ones by modifying the chemical composition (Jiao et al., 2018). The photochemical and microbial processes frequently co-occur in the sunlit ocean, where photochemical reactions modify DOM composition and influence microbial activity through various pathways (Lønborg et al., 2013; Wetzel et al., 2003).

Photobleaching of DOM is associated with a suite of free radicals, such as carboxyl radical, hydroxyl radical and superoxide anion (Mopper et al., 2015; Wei et al., 2023). Generally, aromatic moieties and unsaturated component (e.g., aromatic or unsaturated molecules) are the most photolabile reactants (Gonsior et al., 2009; Stubbins et al., 2010). Upon light absorption, they can lead to the production of bioavailable compounds (e.g., polyols and pyruvate) for microbial further utilization (Gonsior et al., 2014; Kieber et al., 1989). However, a proportion of aromatic compounds can also fuel the growth of specialized bacteria which show alternative inhabitation effects when photochemical processes are active (Nalven et al., 2020; Ward et al., 2017). In some cases, photodegradation can produce biodegradable aromatics that enhance microbial biodegradation of DOM (Bowen et al., 2020; Hu et al., 2023). In addition, photochemical processes can initiate cross-linking, humification and polymerization of labile biomolecules into more recalcitrant compounds that are resistant to microbial degradation (Benner and Biddanda, 1998; Obernosterer et al., 1999). The various effects of photochemical and microbial processes on the DOM pool likely result from their different impacts on the DOM chemical and microbial community composition (Mopper et al., 2015; Ward et al., 2017). Coupled photochemical-microbial degradation regulates carbon cycling and plays a crucial role in marine food web dynamics (Mopper et al., 2015). Fully understanding the combined effects of photodegradation and biodegradation requires knowledge of how these processes influence molecular compositions of DOM and microbial community.

To evaluate the impact of repeated photochemical and microbial processes on DOM chemical composition and microbial communities, we continuously subjected DOM to irradiated or dark conditions followed by inoculation with environmental microorganisms and repeated this in a two-phases experiment. Specifically, we wanted to: (1) identify how irradiation and microbial alteration impact DOM composition; (2) determine which microbial communities thrive when growing on irradiated and non-irradiated substrates; and (3) identify potential links between the microbial community and the DOM chemical composition. During the experiments we characterized changes in the DOM composition by fluorescent spectroscopy, Fourier transform ion cyclotron mass spectrometry (FT-ICR MS) and liquid chromatography coupled to tandem mass spectrometry (LC-MS/MS), while changes in the microbial community was determined by high-throughput sequencing.

2. Materials and methods

2.1. Experimental setup

Our experimental setup included two phases: in the first phase, fresh DOM collected from station S07 close to Xiamen Island, China (~24° N, ~118° E; September 2021) (Fig. S1) was irradiated or kept in the dark for five days and then inoculated with bacteria for an additional five days. In the second phase, DOM subjected to initial irradiation and microbial degradation was further irradiated or kept in the dark for another five days and then inoculated with fresh bacteria for an additional five days.

The initial collected seawater was pre-filtered (mesh size of 20 μm) to remove larger eukaryotic organisms and particles. Subsequently it was filtered using tangential flow filtration with pellicon (0.2 μm, Millipore, USA) to prepare bacterial inoculum and preserved at 4 °C. The filtrate was divided into 2 L quartz glass bottles (acid washed, rinsed with Milli-Q water, and pre-combusted at 450 °C for 6 h) and thereafter either exposed to irradiation in a solar simulation chamber (836 ± 56 μmol $m^{-2}{\cdot}s^{-1}$) or kept in the dark over a five-day period. This light intensity was within average light intensities measured during September in the study area. All treatments remained at 26 °C with thermostatic baths regulating the temperatures. The concentrated "bacterial culture" was thereafter added to the irradiated and non-irradiated treatments in a ratio of 1:9 of the initial microbial abundance and thereafter incubated in the dark for 5 day at room temperature. For the phase II experiment, fresh surface seawater was collected from station GYS near Xiamen Island and treated as described above to create a concentrated bacterial inoculum, which was kept at 4 °C until used. The irradiated treatments from phase I were again filtered by tangential flow filtration. The resulting filtrate was then separated into 2 L quartz glass bottles, which were either irradiated or kept in the dark for another five days. Thereafter the phase II "bacterial culture" was added in a ratio of 1:9 of the initial microbial abundance and incubated in the dark for 5 day at room temperature. In the below we will refer to samples exposed to light as "irradiated" and those kept in the dark as "non-irradiated".

2.2. Sample collection

Triplicate bottles irradiated or kept in the dark were subsampled during phase I (day 5, 7 and 10) and phase II (day 15, 17 and 20) during the incubations. The collected samples include bacterial abundance, microbial community composition, inorganic nutrients, dissolved organic carbon (DOC) concentrations, fluorescent DOM (FDOM), and DOM extraction for chemical analysis. Briefly, 2 mL samples were collected and fixed with glutaraldehyde (1% v/v) and kept at −80 °C for bacterial abundance analysis. In addition, 500 mL of samples were filtered through a 0.22-μm polycarbonate filter (prewashed with 1 L Milli-Q water, Millipore, USA) for microbial community analysis. Subsequently, 20 mL of filtered water samples were stored in two glass vials (CNW, German) at 4 °C for DOC and FDOM analysis, respectively, within three days. Additionally, 40 mL of filtrates were transferred to 50 mL acid cleaned tubes and stored at −20 °C for inorganic nutrient analysis. For the DOM extraction, 400 mL filtrates were acidified to a pH of 2 in a 1 L glass bottle. All glassware used in the experiment was acid washed, rinsed with Milli-Q water, and pre-combusted (450 °C for 6 h).

2.3. Inorganic nutrient and DOM analysis

Concentrations of nitrate + nitrite (NOx) and phosphate (PO_4^{3-}) were determined using a PowerMon Kolorimeter AA3 (Bran + Luebbe, Co., Germany) segment flow analyser, following previously described methods (Knap et al., 1996). While the ammonium (NH_4^+) concentrations were measured using a fluorometric method (Holmes et al., 1999).

The DOC concentrations were determined using a Shimadzu TOC-VCPH analyzer. Briefly, samples were acidified (pH = 2) with phosphoric acid before measurement. The DOC concentrations were calculated by subtracting a Milli-Q water blank and dividing by the slope of a standard curve made from potassium hydrogen phthalate standards.

Excitation (Ex)-emission (Em) matrices (EEMs) were measured using a Horiba Aqualog system. Once the samples reached room temperature, they were excited from 240 to 600 nm with 5 nm intervals using a 1-cm path length quartz cuvette. Emission scans ranged from 248 to 829 nm with 2.33 nm measuring intervals, and each scan had an integration time of 2 s. Parallel factor analysis (PARAFAC) was performed to decompose the data into individual fluorescent components in Matlab (2018) (Murphy et al., 2013). All measured fluorescence intensities of each sample were normalized to Raman Units (RU) with Milli-Q (Ex = 350 nm, Em = 371–428 nm) as a reference (Lawaetz and Stedmon, 2009). The spectral were submitted to the OpenFluor database (https://openfluor.lablicate.com) for source assignment.

Samples (400 mL) for solid phase extraction (SPE) were acidified (pH = 2) and then extracted using cartridges (200 mg, Agilent Bond Elut PPL, USA) as described previously (Dittmar et al., 2008). After extraction, cartridges were eluted with methanol and the estimated SPE extraction efficiency of DOM was ~35%. The FT-ICR MS analysis was

performed using a 9.4 T Bruker Apex Ultra equipped with an Apollo II electrospray ion source operated in negative mode, following previously established protocols (He et al., 2020). The mass peaks with signal-to-noise (s/n) ratios greater than 4 were exported for the formula assignment, and s/n ratio greater than 6 were selected for further analysis. Resolved isotopic species were excluded from further analysis and matched formulas consisted of the elemental combinations of $^{12}C_{1-60}$, $^{1}H_{1-120}$, $^{14}N_{0-3}$, $^{16}O_{0-30}$, and $^{32}S_{0-1}$. Formulas presented in at least two replicates were considered and results were presented as average of three replicates. The relative abundance of identified formulas (CHO, CHON, CHOS and CHONS), and ratios of hydrogen to carbon (H/C) and oxygen to carbon (O/C) were calculated for each sample (Sleighter et al., 2009). Double bond equivalents (DBE) and modified aromaticity index (AI_{mod}) of the identified molecular formulas were calculated as previously described (Koch and Dittmar 2006, 2016). Molecular formulas were assigned to saturated compounds ($H/C > 2$), unsaturated aliphatic compound ($2.0 \geq H/C > 1.5$), lipid-like ($0.2 \geq O/C \geq 0$, $2.2 \geq H/C \geq 1.7$), carbohydrates ($1.2 \geq O/C \geq 0.6$, $2.2 \geq H/C > 1.5$), lignin-like ($0.6 > O/C \geq 0.1$, $1.7 \geq H/C \geq 0.6$, $AI_{mod} < 0.67$), tannin-like ($1.2 \geq O/C \geq 0.6$, $1.5 \geq H/C \geq 0.5$, $AI_{mod} < 0.67$) and condensed aromatics ($1.0 \geq O/C \geq 0$, $0.7 \geq H/C \geq 0.3$, $AI_{mod} \geq 0.67$) (Antony et al., 2014; Seidel et al., 2015). For LC-MS/MS measurement, chromatographic separation was performed on a SHIMADZU-LC30 UHPLC system with a ACQUITY UPLC HSS T3 column (2.1 mm × 150 mm, 1.8 μm, Waters, USA). The eluents were analyzed on a Q Exactive™ plus Hybrid Quadrupole-Orbitrap™ Mass Spectrometer (QE plus, Thermo Fisher Scientific, USA) in heated electrospray ionization positive (3.8 kV spray voltage) and negative (3.2 kV spray voltage) mode. The capillary and probe heater temperatures were 320 and 350 °C, respectively. The sheath gas, aux gas and S-lens RF level were 50 Arb, 15 Arb and 50 Arb. The full scan was operated at a high resolution of 70,000 FWHM ($m/z = 200$) in the range of 80–1200 m/z with an AGC target setting of 3×10^6. Simultaneously, the fragment ion information of the top 10 precursors in each scan was acquired with a mass resolution of 17,500 FWHM, an AGC target of 1×10^5 and the HCD energy at 20, 30 and 40 eV. The accurate m/z of precursors and product ions were matched against online databases including HMDB and MassBank, and an in-house standard library.

2.4. Bacterial abundance and microbial community composition

Bacterial abundance (BA) was determined using flow cytometry (BD Accuri C6). Thawed samples were stained with the nucleic acid-specific dye SYBR Green I (Invitrogen, USA) for 15 min in the dark before measurement (Marie et al., 1997).

The total microbial DNA was extracted from the collected filters using the phenol-chloroform-isoamyl alcohol method as previously described (Wang et al., 2017). For the microbial community structure analysis, bacterial 16S rRNA gene (V4-V5 region) of the DNA samples were amplified using forward primers (515F 5′-GTGCCAGCMGCCGCGGTAA-3′) and reverse primers (907R 5′-CCGTCAATTCMTTTRAGTTT-3′). Quantified amplicons were sequenced by the Illumina MiSeq PE250 platform (Illumina, USA). Analyses of the raw sequences including demultiplexing, denoising and taxonomy classification were performed using the QIIME2 pipeline (Version, 2020.2) with standard parameters (Bolyen et al., 2019). After importing and demultiplexing, sequences were trimmed to 230 bp, and the low-quality sequences were removed (with default parameters). Then the sequences were denoised into amplicon sequence variants (ASVs) using Deblur within QIIME2. The resulting feature table and representative sequences were classified using the QIIME2 pretrained SILVA database classifier (SILVA database release 132). The final dataset contained 2,848,108 sequences constituting 725 ASVs after removing the chloroplast. These ASVs were rarified to 45,571 sequences per sample for α diversity analyses.

2.5. Statistical analysis

Orthogonal projections to latent structures discriminant analysis (OPLS-DA) was conducted to identify metabolites that varied between irradiated and non-irradiated treatments, based on variable important in projection (VIP) values greater than 1. The significance of these metabolites was further tested using TTEST ($p < 0.05$). Selected metabolites were grouped in the heatmap (standardization transformed). Key molecular formulas (top 10 formulas with significant alterations) were identified based on their relative intensity changes (Herzsprung et al., 2023) and principal component analysis (PCA) was applied to investigate the compositional differences of molecular characteristics among key molecules. Microbial community structures (family level) were shown in a circos plot to illustrate the successional changes of dominant microbial community. Alpha-diversity was determined by the Shannon and Pielou indices whose significance was tested by TTEST. Irradiation or non-irradiation adapted microbial community (ASV level) were identified by relative intensity changes with thresholds of $\log_2(FC) > 2$ and TTEST ($p < 0.05$). Mentel test was applied to evaluate the associations between the microbial community and environmental variables. The associations between the microbial community (family level, relative abundance) and key molecules (relative intensity) were presented in the co-occurrence network based on a Spearmen's rank correlation coefficient of $|r| > 0.5$, $p < 0.01$. Corresponding R codes for networks were derived from GitHub (https://github.com/ryanjw/co-occurrence) (Williams et al., 2014). The betweenness and degree indices were calculated to represent the centrality and connectivity of microbial communities and key molecules in the network, respectively. Additionally, molecular mass differences were calculated by subtracting the theoretical mass (theo = 12 × C + 1.007825 × (H−1) + 15.994915 × O + 14.003074 × N + 31.97207 × S) between key molecules (Audi and Wapstra, 1995) and matched to potential functional groups. All statistical analyses were performed in R 3.6.1 (www.R-project.org) using 'statnet', 'circlize', 'ggplot2', 'vegan', 'dplyr', 'ggcor', 'devtools', 'ropls' and 'pheatmap' packages, and network visualizations were conducted in Cytoscape V3.7.2.

3. Results and discussion

3.1. Impacts on dissolved organic carbon, microbial abundance and inorganic nutrients

The initial DOC concentration in phase I was 97.4 ± 7.1 μmol/L, which decreased to 85.8 ± 1.5 and 88.4 ± 2.0 μmol/L in irradiated and non-irradiated treatments, respectively (Fig. S2a). During phase II, DOC concentrations initially increased slightly but then gradually decreased, reaching 83.0 ± 0.1 μmol/L in the irradiated and 86.3 ± 0.2 μmol/L in the non-irradiated treatment by the end. Overall, BA increased in response to DOC consumption. During phase I, BA increased from initially $8.8 \pm 0.8 \times 10^4$ cells/mL to peak of $1.6 \pm 0.1 \times 10^6$ and $8.2 \pm 1.3 \times 10^5$ cells/mL in irradiated and non-irradiated treatments, respectively (Fig. S2b). In phase II, BA increased from $1.5 \pm 0.1 \times 10^5$ cells/mL to peak values of $1.0 \pm 0.2 \times 10^6$ cells/mL in the irradiated and $9.3 \pm 0.2 \times 10^5$ cells/mL in the non-irradiated treatment. It should be noted that a minor bacterial population ($\sim 10^4$ cells/mL) remained after filtration, showing slight growth in the non-irradiated treatment before microbial inoculation. In comparison to the non-irradiated treatment, the irradiated treatment exhibited a relatively higher DOC degradation, which also lead to elevated bacterial abundances in both phases. Overall, irradiation solely, microbial alteration alone, and the combined impact of irradiation and microbial alteration contributed about 1%, 11% and 12%, respectively, to DOC degradation by the end of the experiments.

The inorganic nutrient concentrations showed only slight changes. The NOx concentrations gradually decreased from 11.9 ± 0.1 to 11.6 ± 0.1 μmol/L in both irradiated and non-irradiated treatments (Fig. S2c).

The NH_4^+ concentrations ranged between 0.21 and 1.02 μmol/L, while PO_4^{3-} concentrations remained between 0.78 and 0.85 μmol/L throughout the two-phase experiment (Figs. S2d and e).

3.2. Photodegradation drive fluorescent DOM transformation

Three fluorescent components were identified using PARAFAC analysis (Fig. 1a). Component C1 (Ex/Em wavelengths: 275/321 nm) was defined as protein-like FDOM which is linked to aromatic amino acids that can potentially be available to microbial degradation (Bianchi et al., 2014). Component C2 (Ex/Em wavelengths: 300/387 nm) was similar to microbially derived humic-like component (Chen et al., 2019), whereas the other humic-like component C3 (Ex/Em wavelengths: 350/458 nm) has a terrestrial signature (Du et al., 2021). The fluorescent intensities of the three FDOM components decreased during light process (irradiation) and showed slightly changes after microbial inoculation in the irradiated treatment (irradiation + microbial alteration) in both phases. On the contrary, the fluorescent intensities only exhibited minor changes in the non-irradiated treatment (microbial alteration) except for a pronounced decrease in C1 intensity during phase I.

Irradiation alone contributed to 65%, 72% and 69% of the loss in fluorescent intensities of C1, C2 and C3, respectively, which was very close to the combined effect of irradiation and microbial alteration on C1 (68%), C2 (72%) and C3 (70%). Fluorescent DOM is regarded as highly photo-reactive component, whose bioavailability tends to alter through sunlight mediated processes (Mopper et al., 2015). Photochemical processes have shown the ability to transform complex humic acids, proteins and light-absorbing components into smaller and simpler structures (Miranda et al., 2020). Overall, microbial alteration alone only accounted for 13%, 8% and 8% of the changes in C1, C2 and C3 fluorescence, respectively (Fig. 1b). The decrease in the protein-like component C1 corresponded with the growth in bacterial abundance. This aligns with the general labile nature of C1, which primarily originate from phytoplankton exudates and/or bacterial metabolites that can stimulate bacterial growth (Goto et al., 2017). The humic-like components C2 and C3 increased slightly over time, aligning with their microbial production, which exhibit resistance to further bacterial degradation (Lønborg et al., 2010). Our results highlight photodegradation as a primary driver in the transformation of FDOM components.

3.3. Biodegradation drive key organic molecular transformation

A summary of molecular characteristics of DOM molecules identified by FT-ICR MS were shown in Table S1. Generally, DBE and AI_{mod} values were lower in the irradiated (8.075 ± 0.043 and 0.218 ± 0.004) compared to non-irradiated (8.137 ± 0.046 and 0.221 ± 0.002) treatment. This indicates that the molecular composition exhibited a relatively lower level of unsaturation and aromaticity after irradiation. This finding is consistent with recent studies showing that photochemical processes are typically linked with the decarboxylation of carboxyl functional groups or rupture of phenolic functional groups (Wei et al., 2023), thereby producing saturated aliphatic compounds (Milstead et al., 2023; Yin et al., 2023). These transformations generally result in a decrease in the molecular unsaturation and aromaticity.

The relative changes in molecular intensity have been applied to identify the key molecular formulas and track molecular transformation process (Herzsprung et al., 2023). Similarly, we characterized the degraded or produced key molecules (top 10 formulas with significant alterations) during light process (irradiation) and subsequently microbial inoculation in the irradiated treatment (irradiation + microbial alteration), as well as in the non-irradiated treatment (microbial alteration) (Fig. 2). The irradiation process led to contrariwise impacts on molecular markers in the two phases. For example, lignin-like markers were produced in phase I but degraded in phase II. This difference may be related to the compounds present, with freshly collected seawater in phase I, while additional bacterial metabolites being present in phase II. Previous studies indicate that lignin-like compounds sourced from aquatic environments are susceptible to photodegradation (Stubbins and Dittmar 2015; Stubbins et al., 2010). However, lignin-like compounds can also increase when pyrogenic or macrophyte-derived DOM is exposed to irradiation (Song et al., 2022). These previous are supported by our results showing that lignin-like compounds can be

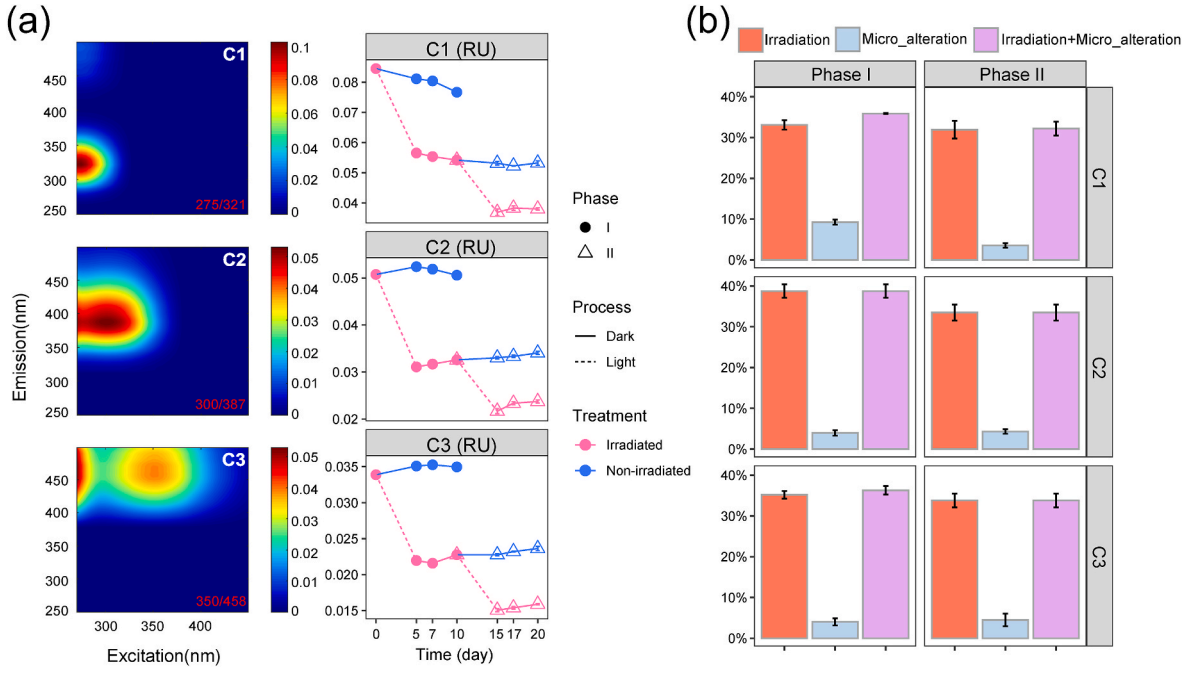

Fig. 1. Changes of the fluorescence components (in Raman units (RU)) (a) over the experimental period. Here component C1 is protein-like components, and components C2 and C3 are humic-like components. Fluorescence intensity changes (b) under irradiation or microbial alteration (micro_alteration) or both (irradiation + micro_alteration).

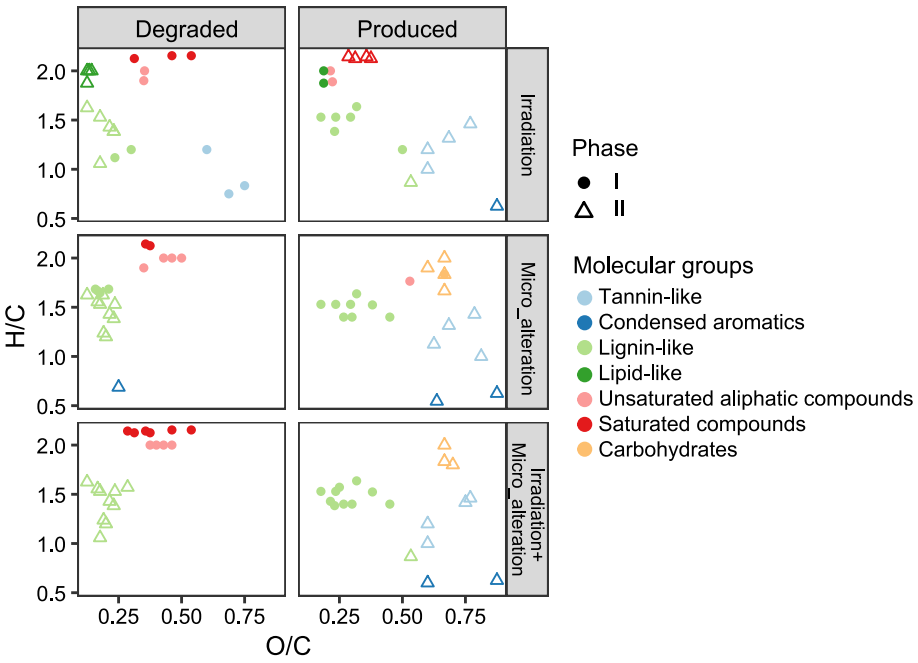

Fig. 2. Van Krevelen diagrams showing degraded or produced key molecules (top 10 formulas with significant alterations) due to irradiation or microbial alteration (micro_alteration) or both (irradiation + micro_alteration).

degraded or produced by light, depending on the substrate compositions. Similarly, aliphatic compounds can decrease due to photodecarboxylation following irradiation (Wei et al., 2023) or they may be produced as irradiation byproducts (Gonsior et al., 2014; Stubbins and Dittmar 2015). In addition to cleaving aromatic molecules, photochemical processes have also been shown to increase the aromaticity of compound, leading to a more recalcitrant nature of the DOM pool (Hu et al., 2023). These previous results align with our findings showing that biologically recalcitrant compounds, such as tannin-like and condensed aromatics, were degraded in phase I but produced in phase II. However, further exploration is needed to understand the specific mechanism by which irradiation affects different molecules and functional groups.

Interestingly, microbial alteration alone and the combined impact of irradiation and microbial alteration exhibited similar patterns in the transformation of key molecules (Fig. 2). Both microbial alteration and combined impact of irradiation and microbial alteration degraded hydrogen (positive correlated with H/C) while producing unsaturated and aromatic (positive correlated with DBE and AImod) molecules in phase I, then further degraded molecules with these characteristics and produced oxidized (positive correlated O/C) formulas in phase II (Fig. S3). However, irradiation alone degraded oxidized while producing hydrogen formulas in phase I, then further degraded reduced (negative correlated with O/C) molecules and produced oxidized formulas in phase II. This result suggests that biological processes play a more significant role than photochemical processes in driving the changes of these key molecules. During phase I, both microbial and combined processes led to the degradation of unsaturated aliphatic and saturated compounds, along with the production of lignin-like compounds. The degraded and produced markers could be distinguished by a molecular labile boundary (H/C = 1.5) and a notable difference in aromaticity (0.02 ± 0.04 vs 0.16 ± 0.10), consistent with bacterial preference for utilizing more labile and less aromatic compounds (Chen et al., 2021; D'Andrilli et al., 2015). In phase II, the lignin-like compounds were further degraded, while tannin-like compounds, carbohydrates and condensed aromatics were produced. During this second experimental phase, the O/C values were lower in the degraded key molecules (0.20 ± 0.05) compared to produced key molecules (0.68 ± 0.09), suggesting microbial production of oxidized compounds. A previous study demonstrated that tannin-like compounds and condensed aromatics with polyphenolic and/or carboxylic acid functional groups are highly oxidized and generally resistant to bacterial degradation (Cai and Jiao, 2023), which could explain their enrichment in phase II. Carbohydrates are generally considered labile compounds which are preferentially degraded by bacteria (Moran et al., 2016). In our experiment, produced carbohydrates were only detected during phase II in the treatments where bacteria were present. This production can be attributed to bacterial transformation process, such as bacterial secondary metabolites or exopolysaccharide derivatives. Overall, we observed different molecular transformation patterns between irradiation, microbial alteration, and the combined impact of irradiation and microbial alteration based on formula composition, despite the absence of structural information.

3.4. *Structural shifts of metabolites under irradiation and biodegradation*

A total of 320 metabolites were further identified by LC-MS/MS to access structural composition shifts in organic compounds. Metabolic compound compositions from irradiated and non-irradiated treatments were grouped into separate clusters in the OPLS-DA plot (Fig. S4a). Different metabolites were categorized into irradiated enriched (n = 17) and non-irradiated enriched (n = 13) groups based on their significant changes (VIP >1 and $p < 0.05$) with or without irradiation process (Figs. S4b and c). The enriched metabolites in either irradiated or non-irradiated treatment were well-clustered in the heatmap (Fig. 3). In the irradiated treatment, aliphatic compounds were enriched, while alicyclic compounds were more abundant in the non-irradiated treatment. This result implies that ring compounds potentially have undergone photodegradation, resulting in the formation or relative increase of linear compounds. Alicyclic compounds such as carboxylic-rich alicyclic molecules are highly sensitive to irradiation, with aliphatic compounds being predominant photodegradation products (Stubbins and Dittmar 2015; Stubbins et al., 2010). Photochemically produced compounds consist of bioavailable polyols and carboxylic acid (Gonsior et al., 2014) which likely explain the enriched organic alcohol (i.e. hexaethylene glycol and lauryl diethanolamide) and organic acid (i.e. sebacic acid and azelaic acid) after irradiation and then gradually consumed during

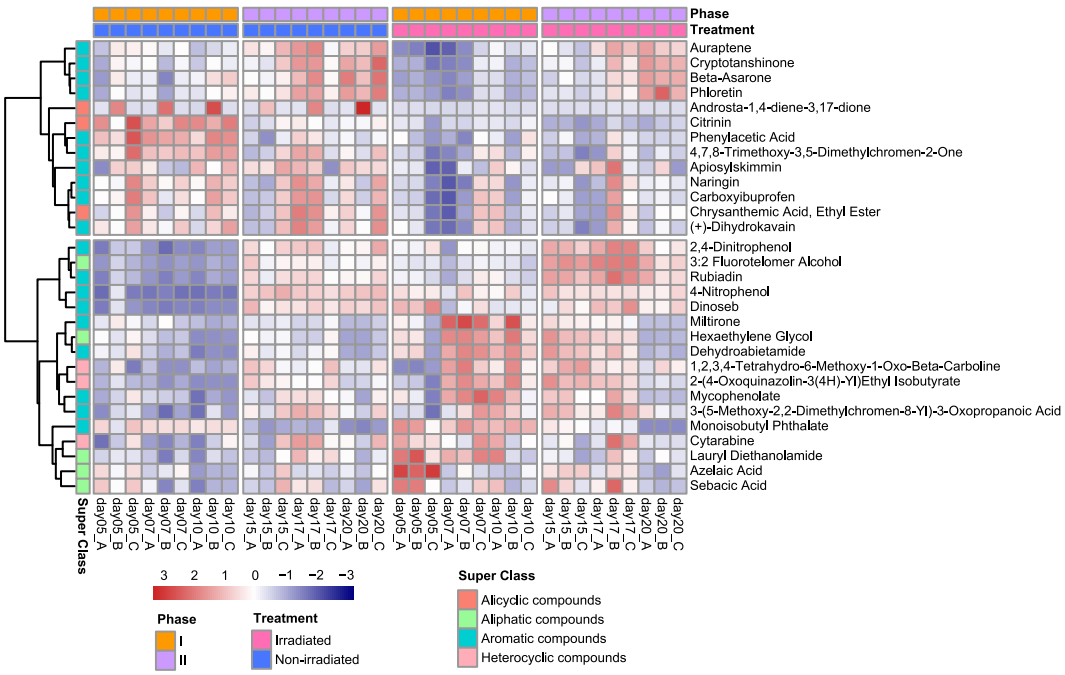

Fig. 3. Heatmap illustrating significantly changed metabolites in the irradiated and non-irradiated treatments.

microbial degradation (Fig. 3 and S4c).

Non-heterocyclic aromatic compounds containing carboxyl/ester functional groups were more enriched in non-irradiated (6 out of 10) compared to irradiated treatment (3 out of 9) (Fig. S4c). Previous studies have recognized these aromatic compounds with higher unsaturation or condensed aromatics as the most photoreactive structural compounds (Gonsior et al., 2009; Stubbins et al., 2010). Photodegradation of aromatic compounds follows an order of functionality loss, with a preference for carboxyl/amide/ester groups (Thorn et al., 2010). Our results, combined with these previous findings, confirm the high propensity of carboxyl/ester aromatics for photochemical alteration. Alternatively, the enrichment of aromatic compounds containing carboxyl/ester functional groups can also be attributed to microbial transformation in the non-irradiated treatment. Additionally, heterocyclic compounds (i.e., nitrogen-containing compounds) along with nitrogen-containing aliphatics and aromatics were exclusively enriched in the irradiated treatment. These nitrogen-containing compounds may have been formed via the dearomatization of heterocyclic precursors during photodegradation (Li et al., 2024). The presence of amide-nitrogen has been linked to labile high molecular weight compounds, whereas prevailed heterocyclic-nitrogen in low molecular weight compounds is mainly biologically recalcitrant (Broek et al., 2023). Our results demonstrate the importance of photochemical processes in the organic nitrogen cycle, as well as the irradiation mediated cross-linking of compounds between labile and recalcitrant forms. It should be noted that the enrichment of structural differences in organic compounds can also be influenced by distinct functional microbial communities under irradiated or non-irradiated treatments.

3.5. Irradiation impacts on microbial successions and alpha-diversity

Microbial diversity was determined by Shannon and Pielou indices, corresponding to microbial diversity and evenness (Fig. 4a). Both Shannon and Pielou indices were significantly higher in the irradiated compared to non-irradiated treatment at the end of phase I ($p_{Shannon}< 0.05$; $p_{Pielou}< 0.05$) and phase II ($p_{Shannon}< 0.01$; $p_{Pielou}< 0.05$). This finding indicates that irradiated substrates support a higher diversity and evenness of the microbial community. The changes induced by irradiation in both fluorescent and molecular organic compounds (Figs. 1–3) likely led to the production of new substrates which could support specific microbial populations (Finke and Snyder, 2008). For example, irradiation exclusively produced lipid-like and saturated compounds (Fig. 2) can increase bioavailability of substrates which may support microbial utilization (D'Andrilli et al., 2015).

The circos plot illustrated the successional changes in microbial community in the irradiated and non-irradiated treatments (Fig. 4b). On average, the relative abundance of *Nitrincolaceae* (20.6% vs 4.4%), *Methylophagaceae* (14.9% vs 4.9%), *Methylophilaceae* (6.3% vs 1.0%) and *Cellvibrionaceae* (3.2% vs 1.0%) were higher in the irradiated treatment. Conversely, *Flavobacteriaceae* (27.4% vs 2.4%), *Alteromonadaceae* (17.0% vs 2.7%) and *Marinobacteraceae* (7.0% vs 2.0%) were enriched in the non-irradiated treatment. *Rhodobacteraceae* (25.6% vs 25.4%) remained similar levels in both treatments. During phase I, the responsive microbes in freshly collected seawater included *Nitrincolaceae* (up to 57.4%) in the irradiated and *Alteromonadaceae* (up to 51.3%) in the non-irradiated treatment, both belonging to *Gammaproteobacteria*. Their opportunistic lifestyles and metabolic versatility enable them to rapid grow when fresh labile organic matter is available (Landa et al., 2013; Teeling et al., 2012). During phase II, *Methylophagaceae* (up to 42.5%) in the irradiated and *Flavobacteriaceae* (up to 57.2%) in the non-irradiated treatment actively responded to the bacterial secondary metabolites/semi-labile compounds from phase I. Methylotrophs are known for their abilities to utilize one-carbon compounds, such as methanol and methylamine (Nercessian et al., 2005; Neufeld et al., 2007). Photodegradation products (e.g., the photooxidation of glycerol) are potential source of these one-carbon compounds (Kumar et al., 2023), thus supporting the growth of *Methylophagaceae* in the irradiated treatment. The successional dominance of *Flavobacteriaceae* in the non-irradiated treatment could be attributed to their various hydrolytic enzymes, which can facilitate the degradation of metabolites derived from *Alteromonadaceae* (Zheng et al., 2018) particularly bacterial exopolysaccharides (Zhang et al., 2015).

Individual ASVs were further classified into irradiation adapted or non-irradiation adapted microbial communities based on significant changes in relative abundance ($\log_2(FC) > 2, p < 0.05$) (Fig. 4c and S5). The irradiation adapted microbial community included *Methylophagaceae*, *Nitrincolaceae* and *Rhodobacteraceae*, whose average abundance increased about 6 folds in the irradiated compared to the non-

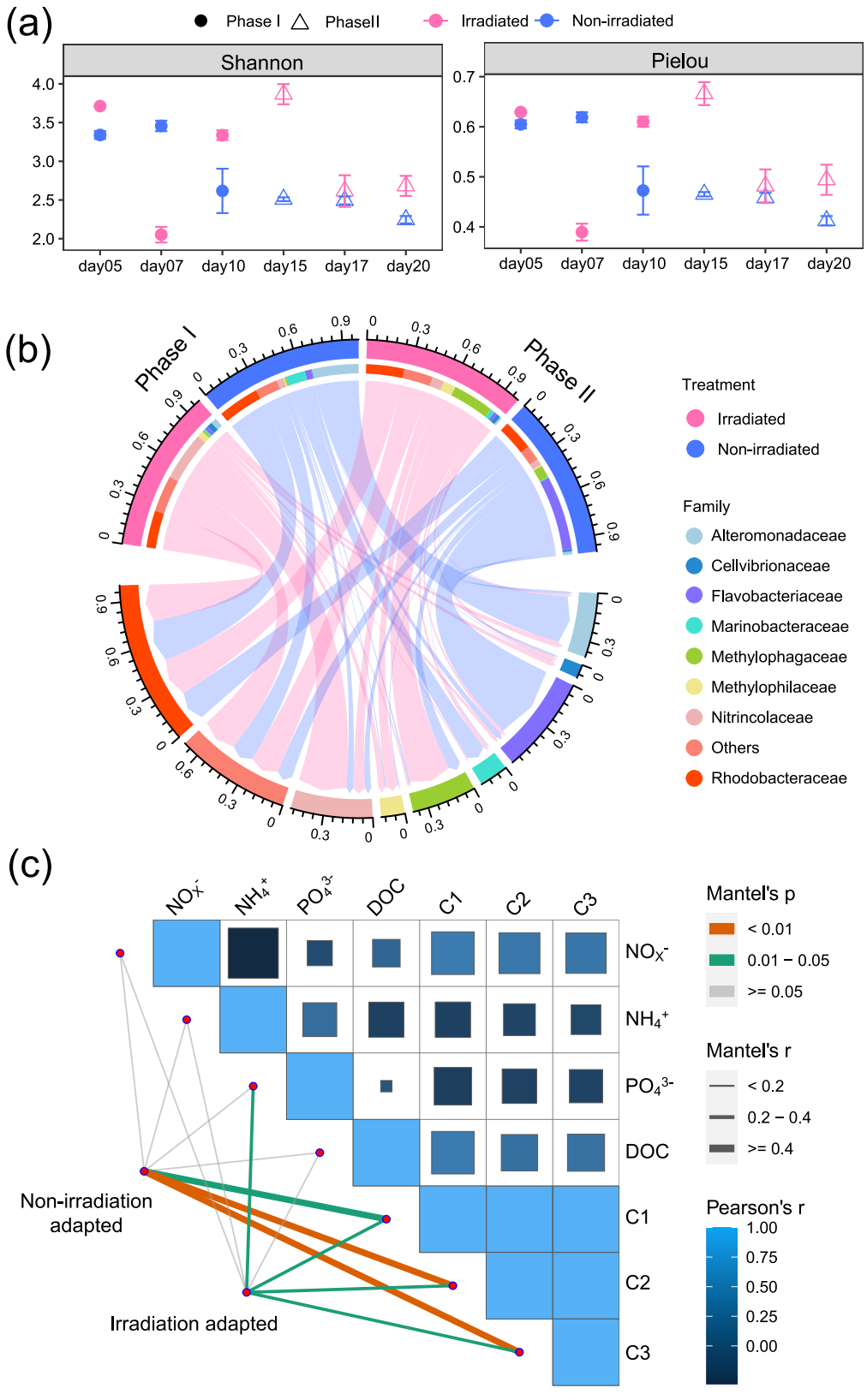

Fig. 4. Changes in microbial diversity (a) and circos plot of the microbial community compositions (b) in irradiated or non-irradiated treatments. Associations between the adapted microbial community under irradiated and non-irradiated conditions and environmental variables (c).

irradiated treatments (Fig. S5). In contrast, the non-irradiation adapted microbial community dominated by *Flavobacteriaceae* and *Marinobacteraceae*, whose average abundance enriched about 17 folds in the non-irradiated compared to the irradiated treatments. The irradiation adapted microbial community was negatively correlated with all three fluorescent components, which were degraded by irradiation (Fig. 4c). This suggests that photodegradation products from fluorescent components may favour the growth of an irradiation adapted microbial community. On the other hand, the C1 FDOM component negatively correlated with non-irradiation adapted microbial community, suggesting potential utilization of C1 for growth. In contrast, the positive correlations between non-irradiation adapted microbial community and humic-like components (C2 and C3) implies potential microbial production of relatively recalcitrant components. This result is consistent with previous incubation experiments demonstrating bacterial utilization of protein-like fluorophores and production of humic-like fluorophores (Zheng et al., 2019).

3.6. Potential transformation between the microbial community and key molecules

Network analysis based on a Spearmen's rank correlation was conducted to investigate potential interactions between the microbial community and key molecules (Fig. 5a). Both *Methylophagaceae* (relative abundance 10%) and *Alteromonadaceae* (10%) had the highest betweenness and degree values representing their important roles in connecting key molecules nodes and facilitating the potential transformation across the networks (Table S2). These key molecules were also linked based on their molecular mass difference which matched different functional group. *Methylophagaceae* was associated with more labile molecules such as saturated compounds and unsaturated aliphatic compounds (Fig. 5a). These key molecules were predominantly linked by mass differences of CH_2 groups (Fig. 5b and Table S2), suggesting that *Methylophagaceae* may transform those key molecules through (de) methylation processes. Methylotrophs are capable of growing on one carbon compounds (e.g., methanol and methylated nitrogen/sulfur compounds), as well as on multi-carbon substrates (Shmareva et al., 2018). Recent studies have also demonstrated that *Methylophagaceae* rapidly respond to aliphatic hydrocarbons (Chen et al., 2020; Doyle et al., 2018). Our results further support these findings by showing that *Methylophagaceae* growth is favoured by irradiated substrates and that potential (de)methylation activities are correlated with their presence.

In contrast, non-irradiation adapted *Alteromonadaceae* were linked with recalcitrant molecules (e.g. tannin-like and condensed aromatics)

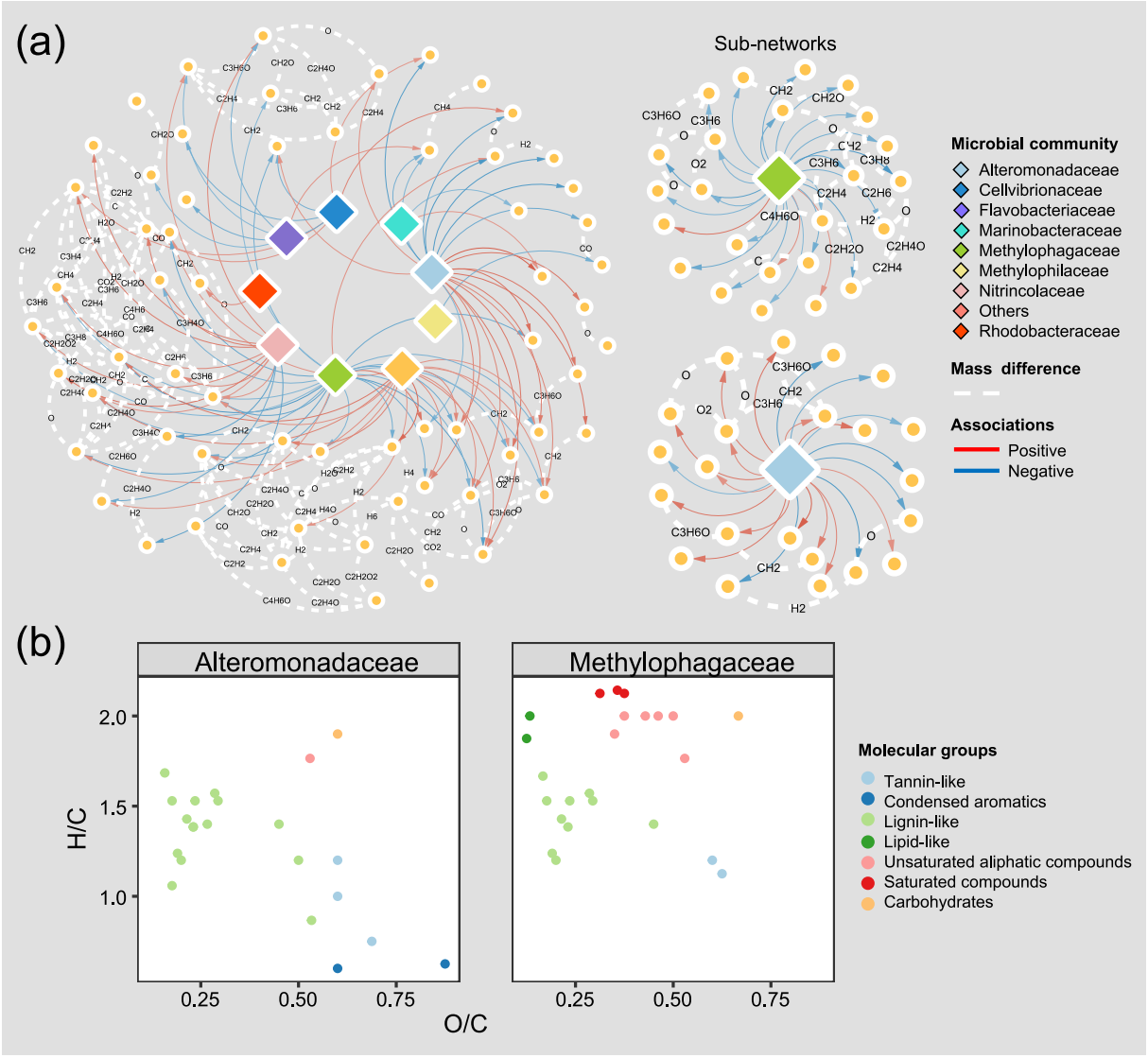

Fig. 5. The co-occurrence network between the microbial community and key molecules (Spearman $|r| > 0.5$, $p < 0.01$) and mass difference among key molecules (a). The van Krevelen diagrams showing the microbial groups associated with the molecular composition (b).

(Fig. 5b). In particular, we observed an increase in molecules that differed by O species (Fig. 5a), indicating that potential (de)oxidation reactions might be important to the formation of recalcitrant DOM by *Alteromonadaceae*. The type strain of *Alteromonadaceae*, *Alteromonas macleodii*, has been shown to decrease molecular oxygen fractions in the short term (36 h) but increase molecular oxygen content over longer periods (60 days) when degrading various photosynthates (Chen et al., 2022; Koch et al., 2019). These findings suggest a partial molecular transformation potentially involving (de)oxidation by *Alteromonadaceae*. Overall, our study highlights the important role of *Methylophagaceae* and *Alteromonadaceae* in the potential transformation of various key molecules. The complementary substrate associations of different microbes under light and dark circles facilitate the utilization and transformation of organic compounds.

4. Conclusion

We investigated the effects of repeated cycles of photodegradation and biodegradation on the composition of DOM and the consequent microbial community (Fig. 6). Photochemical processes primarily altered protein- and humic-like fluorophores, whereas microbial processes dominated the transformation of key molecules. Photochemical processes increased the presence of aliphatic and nitrogen-containing compounds, and enhanced microbial diversity. In contract microbial degradation enriched the DOM pool with alicyclic compounds and aromatic compounds containing carboxyl/ester functional groups. Correlation analyses that evaluated the responses of microbial communities indicated that *Methylophagaceae* (irradiation adapted) and *Alteromonadaceae* (non-irradiation adapted) were key taxa that left an imprint on DOM composition. Our study highlights that a sector of plankton microbial communities is apparently specialized for metabolizing DOM that has been altered by photodegradation. Moreover, we show that the fate of DOM exposed in highly illuminated surface layers is partly determined by a complex but poorly determined interaction between light-driven abiotic processes and heterotrophic plankton microbial communities.

CRediT authorship contribution statement

Qi Chen: Writing – review & editing, Writing – original draft, Visualization, Methodology, Investigation, Formal analysis. **Christian Lønborg:** Writing – review & editing, Investigation, Formal analysis,

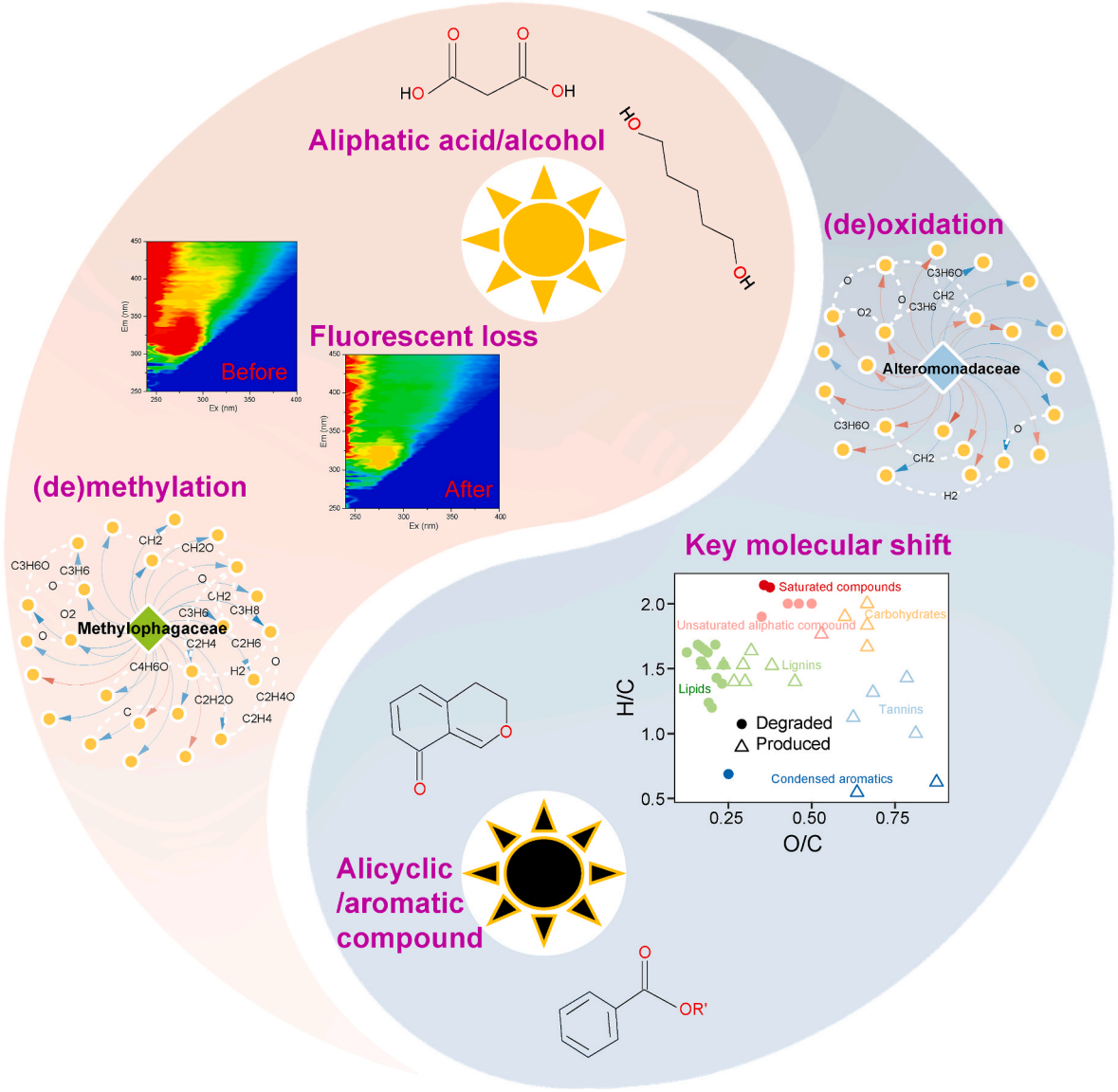

Fig. 6. Schematic summarizing selective impacts of photochemical and microbial processes on marine dissolved organic matter pool and microbes.

Conceptualization. **Jiaxin Chen:** Writing – review & editing, Methodology, Investigation. **Stephen J. Giovannoni:** Writing – review & editing, Supervision, Conceptualization. **Chen He:** Writing – review & editing, Software. **Kunshan Gao:** Writing – review & editing, Methodology. **Quan Shi:** Writing – review & editing, Validation. **Nianzhi Jiao:** Writing – review & editing, Supervision, Resources, Project administration. **Qiang Zheng:** Writing – review & editing, Supervision, Resources, Project administration, Conceptualization.

Declaration of competing interest

The authors declare that they have no known competing financial interests or personal relationships that could have appeared to influence the work reported in this paper.

Acknowledgments

This work was supported by National Natural Science Foundation of China (42222604 and 42188102), National Key R&D Program of China (2024YFF0507000), the Independent Research Fund Denmark (Grant No. 1127-00033B) and the MEL senior visiting fellowship program (Xiamen University, China).

Appendix A. Supplementary data

Supplementary data to this article can be found online at https://doi.org/10.1016/j.envres.2025.121159.

Data availability

Sequence data were deposited in the National Center for Biotechnology Information (NCBI) Sequence Read Archive with BioProject PRJNA1129106. FT-ICR MS data were deposited on figshare (https://doi.org/10.6084/m9.figshare.26112376).

References

Antony, R., Grannas, A.M., Willoughby, A.S., Sleighter, R.L., Thamban, M., Hatcher, P.G., 2014. Origin and sources of dissolved organic matter in snow on the East Antarctic ice sheet. Environ. Sci. Technol. 48 (11), 6151–6159. https://doi.org/10.1021/es405246a.

Audi, G., Wapstra, A.H., 1995. The 1995 update to the atomic mass evaluation. Nucl. Phys. 595 (4), 409–480. https://doi.org/10.1016/0375-9474(95)00445-9.

Azam, F., Fenchel, T., Field, J.G., Gray, J.S., Meyerreil, L.A., Thingstad, F., 1983. The ecological role of water-column microbes in the sea. Mar. Ecol. Prog. Ser. 10 (3), 257–263. https://doi.org/10.3354/meps010257.

Bar-On, Y.M., Milo, R., 2019. The biomass composition of the oceans: a blueprint of our blue planet. Cell 179 (7), 1451–1454. https://doi.org/10.1016/j.cell.2019.11.018.

Benner, R., Biddanda, B., 1998. Photochemical transformations of surface and deep marine dissolved organic matter: effects on bacterial growth. Limnol. Oceanogr. 43 (6), 1373–1378. https://doi.org/10.4319/lo.1998.43.6.1373.

Bianchi, T.S., Osburn, C., Shields, M.R., Yvon-Lewis, S., Young, J., Guo, L.D., et al., 2014. Deepwater horizon oil in gulf of Mexico waters after 2 Years: transformation into the dissolved organic matter pool. Environ. Sci. Technol. 48 (16), 9288–9297. https://doi.org/10.1021/es501547b.

Bolyen, E., Rideout, J.R., Dillon, M.R., Bokulich, N.A., Abnet, C.C., Al-Ghalith, G.A., et al., 2019. Reproducible, interactive, scalable and extensible microbiome data science using QIIME 2. Nat. Biotechnol. 37 (8), 852–857. https://doi.org/10.1038/s41587-019-0209-9.

Bowen, J.C., Kaplan, L.A., Cory, R.M., 2020. Photodegradation disproportionately impacts biodegradation of semi-labile DOM in streams. Limnol. Oceanogr. 65 (1), 13–26. https://doi.org/10.1002/lno.11244.

Broek, T.A.B., McCarthy, M.D., Ianiri, H.L., Vaughn, J.S., Mason, H.E., Knapp, A.N., 2023. Dominant heterocyclic composition of dissolved organic nitrogen in the ocean: a new paradigm for cycling and persistence. Proc. Natl. Acad. Sci. U. S. A 120 (49), e2305763120. https://doi.org/10.1073/pnas.2305763120.

Cai, R., Jiao, N., 2023. Recalcitrant dissolved organic matter and its major production and removal processes in the ocean. Deep Sea Research Part II 191, 103922. https://doi.org/10.1016/j.dsr.2022.103922.

Carlson, C.A., Hansell, D.A., 2015. DOM Sources, Sinks, Reactivity, and Budgets, pp. 65–126.

Chen, Q., Chen, F., Gonsior, M., Li, Y., Wang, Y., He, C., et al., 2021. Correspondence between DOM molecules and microbial community in a subtropical coastal estuary on a spatiotemporal scale. Environ. Int. 154, 106558. https://doi.org/10.1016/j.envint.2021.106558.

Chen, Q., Lonborg, C., Chen, F., Gonsior, M., Li, Y.Y., Cai, R.H., et al., 2022. Increased microbial and substrate complexity result in higher molecular diversity of the dissolved organic matter pool. Limnol. Oceanogr. 67 (11), 2360–2373. https://doi.org/10.1002/lno.12206.

Chen, Q.G., Bao, B., Li, Y.J., Liu, M., Zhu, B.K., Mu, J., et al., 2020. Effects of marine oil pollution on microbial diversity in coastal waters and stimulating indigenous microorganism bioremediation with nutrients. Regional Studies in Marine Science 39, 101395. https://doi.org/10.1016/j.rsma.2020.101395.

Chen, S., Lu, Y., Dash, P., Das, P., Li, J., Capps, K., et al., 2019. Hurricane pulses: small watershed exports of dissolved nutrients and organic matter during large storms in the Southeastern USA. Sci. Total Environ. 689, 232–244. https://doi.org/10.1016/j.scitotenv.2019.06.351.

D'Andrilli, J., Cooper, W.T., Foreman, C.M., Marshall, A.G., 2015. An ultrahigh-resolution mass spectrometry index to estimate natural organic matter lability. Rapid Commun. Mass Spectrom. 29 (24), 2385–2401. https://doi.org/10.1002/rcm.7400.

Dittmar, T., Koch, B., Hertkorn, N., Kattner, G., 2008. A simple and efficient method for the solid-phase extraction of dissolved organic matter (SPE-DOM) from seawater. Limnol Oceanogr. Methods 6 (6), 230–235. https://doi.org/10.4319/lom.2008.6.230.

Doyle, S.M., Whitaker, E.A., De Pascuale, V., Wade, T.L., Knap, A.H., Santschi, P.H., et al., 2018. Rapid Formation of microbe-oil aggregates and changes in community composition in coastal surface water following exposure to oil and the dispersant corexit. Front. Microbiol. 9, 689. https://doi.org/10.3389/fmicb.2018.00689.

Du, Y., Lu, Y., Roebuck Jr., J.A., Liu, D., Chen, F., Zeng, Q., et al., 2021. Direct versus indirect effects of human activities on dissolved organic matter in highly impacted lakes. Sci. Total Environ. 752, 141839. https://doi.org/10.1016/j.scitotenv.2020.141839.

Gonsior, M., Hertkorn, N., Conte, M.H., Cooper, W.J., Bastviken, D., Druffel, E., et al., 2014. Photochemical production of polyols arising from significant photo-transformation of dissolved organic matter in the oligotrophic surface ocean. Mar. Chem. 163, 10–18. https://doi.org/10.1016/j.marchem.2014.04.002.

Gonsior, M., Peake, B.M., Cooper, W.T., Podgorski, D., D'Andrilli, J., Cooper, W.J., 2009. Photochemically induced changes in dissolved organic matter identified by ultrahigh resolution fourier transform ion cyclotron resonance mass spectrometry. Environ. Sci. Technol. 43 (3), 698–703. https://doi.org/10.1021/es8022804.

Goto, S., Tada, Y., Suzuki, K., Yamashita, Y., 2017. Production and reutilization of fluorescent dissolved organic matter by a marine bacterial strain, Alteromonas macleodii. Front. Microbiol. 8, 507. https://doi.org/10.3389/fmicb.2017.00507.

Hansell, D.A., Carlson, C.A., Repeta, D.J., Schlitzer, R., 2009. Dissolved organic matter in the ocean a controversy stimulates new insights. Oceanography (Wash., D.C.) 22 (4), 202–211. https://doi.org/10.5670/oceanog.2009.109.

Harrison, J.A., Caraco, N., Seitzinger, S.P., 2005. Global patterns and sources of dissolved organic matter export to the coastal zone: results from a spatially explicit, global model. Glob. Biogeochem. Cycles 19 (4). https://doi.org/10.1029/2005gb002480.

He, C., Zhang, Y., Li, Y., Zhuo, X., Li, Y., Zhang, C., et al., 2020. In-house standard method for molecular characterization of dissolved organic matter by FT-ICR mass spectrometry. ACS Omega 5 (20), 11730–11736. https://doi.org/10.1021/acsomega.0c01055.

Herzsprung, P., Kamjunke, N., Wilske, C., Friese, K., Boehrer, B., Rinke, K., et al., 2023. Data evaluation strategy for identification of key molecular formulas in dissolved organic matter as proxies for biogeochemical reactivity based on abundance differences from ultrahigh resolution mass spectrometry. Water Res. 232, 119672. https://doi.org/10.1016/j.watres.2023.119672.

Holmes, R.M., Aminot, A., Kerouel, R., Hooker, B.A., Peterson, B.J., 1999. A simple and precise method for measuring ammonium in marine and freshwater ecosystems. Can. J. Fish. Aquat. Sci. 56 (10), 1801–1808. https://doi.org/10.1139/cjfas-56-10-1801.

Holt, A.D., Kellerman, A.M., Li, W.B., Stubbins, A., Wagner, S., McKenna, A., et al., 2021. Assessing the role of photochemistry in driving the composition of dissolved organic matter in glacier runoff. Journal of Geophysical Research-Biogeosciences 126 (12), e2021JG006516. https://doi.org/10.1029/2021JG006516.

Hu, J., Kang, L., Li, Z., Feng, X., Liang, C., Wu, Z., et al., 2023. Photo-produced aromatic compounds stimulate microbial degradation of dissolved organic carbon in thermokarst lakes. Nat. Commun. 14 (1), 3681. https://doi.org/10.1038/s41467-023-39432-2.

Jiao, N., Herndl, G.J., Hansell, D.A., Benner, R., Kattner, G., Wilhelm, S.W., et al., 2010. Microbial production of recalcitrant dissolved organic matter: long-term carbon storage in the global ocean. Nat. Rev. Microbiol. 8 (8), 593–599. https://doi.org/10.1038/nrmicro2386.

Jiao, N., Robinson, C., Azam, F., Thomas, H., Baltar, F., Dang, H., et al., 2014. Mechanisms of microbial carbon sequestration in the ocean – future research directions. Biogeosciences 11 (19), 5285–5306. https://doi.org/10.5194/bg-11-5285-2014.

Jiao, N.Z., Cai, R.H., Zheng, Q., Tang, K., Liu, J.H., Jiao, F.L.E., et al., 2018. Unveiling the enigma of refractory carbon in the ocean. Natl. Sci. Rev. 5 (4), 459–463. https://doi.org/10.1093/nsr/nwy020.

Kieber, D.J., Mcdaniel, J., Mopper, K., 1989. Photochemical source of biological substrates in sea-water - implications for carbon cycling. Nature 341 (6243), 637–639. https://doi.org/10.1038/341637a0.

Knap, A., Michaels, A., Close, A., Ducklow, H., Dickson, A., 1996. Protocols for the Joint Global Ocean Flux Study (JGOFS) Core Measurements.

Koch, B., Dittmar, T., 2016. Erratum: from mass to structure: an aromaticity index for high-resolution mass data of natural organic matter. Rapid Commun. Mass Spectrom. 30, 250.

Koch, B.P., Dittmar, T., 2006. From mass to structure: an aromaticity index for high-resolution mass data of natural organic matter. Rapid Commun. Mass Spectrom. 20 (5), 926–932. https://doi.org/10.1002/rcm.2386.

Koch, H., Durwald, A., Schweder, T., Noriega-Ortega, B., Vidal-Melgosa, S., Hehemann, J.H., et al., 2019. Biphasic cellular adaptations and ecological implications of Alteromonas macleodii degrading a mixture of algal polysaccharides. ISME J. 13 (1), 92–103. https://doi.org/10.1038/s41396-018-0252-4.

Kumar, M., Meena, B., Yu, A.M., Sun, C.H., Challapalli, S., 2023. Advancements in catalysts for glycerol oxidation photo-/electrocatalysis: a comprehensive review of recent developments. Green Chem. 25 (21), 8411–8443. https://doi.org/10.1039/d3gc03094f.

Landa, M., Cottrell, M.T., Kirchman, D.L., Blain, S., Obernosterer, I., 2013. Changes in bacterial diversity in response to dissolved organic matter supply in a continuous culture experiment. Aquat. Microb. Ecol. 69 (2), 157. https://doi.org/10.3354/ame01632.

Lawaetz, A.J., Stedmon, C.A., 2009. Fluorescence intensity calibration using the Raman scatter peak of water. Appl. Spectrosc. 63 (8), 936–940. https://doi.org/10.1366/000370209788964548.

Li, S., Harir, M., Bastviken, D., Schmitt-Kopplin, P., Gonsior, M., Enrich-Prast, A., et al., 2024. Dearomatization drives complexity generation in freshwater organic matter. Nature 628 (8009), 776–781.

Li, S., Hou, X., Shi, Y., Huang, T., Yang, H., Huang, C., 2020. Rapid photodegradation of terrestrial soil dissolved organic matter (DOM) with abundant humic-like substances under simulated ultraviolet radiation. Environ. Monit. Assess. 192 (2), 103. https://doi.org/10.1007/s10661-019-7945-7.

Lønborg, C., Álvarez-Salgado, X.A., Davidson, K., Martínez-García, S., Teira, E., 2010. Assessing the microbial bioavailability and degradation rate constants of dissolved organic matter by fluorescence spectroscopy in the coastal upwelling system of the Ría de Vigo. Mar. Chem. 119 (1–4), 121–129. https://doi.org/10.1016/j.marchem.2010.02.001.

Lønborg, C., Martínez-García, S., Teira, E., Álvarez-Salgado, X.A., 2013. Effects of the photochemical transformation of dissolved organic matter on bacterial physiology and diversity in a coastal system. Estuar. Coast Shelf Sci. 129, 11–18. https://doi.org/10.1016/j.ecss.2013.05.013.

Marie, D., Partensky, F., Jacquet, S., Vaulot, D., 1997. Enumeration and cell cycle analysis of natural populations of marine picoplankton by flow cytometry using the nucleic acid stain SYBR green I. Appl. Environ. Microbiol. 63 (1), 186–193. https://doi.org/10.1128/aem.63.1.186-193.1997.

Milstead, R.P., Horvath, E.R., Remucal, C.K., 2023. Dissolved organic matter composition determines its susceptibility to complete and partial photooxidation within lakes. Environ. Sci. Technol. 57 (32), 11876–11885. https://doi.org/10.1021/acs.est.3c01500.

Miranda, M.L., Osterholz, H., Giebel, H.A., Bruhnke, P., Dittmar, T., Zielinski, O., 2020. Impact of UV radiation on DOM transformation on molecular level using FT-ICR-MS and PARAFAC. Spectrochim. Acta Mol. Biomol. Spectrosc. 230, 118027. https://doi.org/10.1016/j.saa.2020.118027.

Mopper, K., Kieber, D.J., Stubbins, A.J.B., 2015. Marine Photochemistry of Organic Matter: Processes and Impacts, pp. 389–450.

Moran, M.A., Ferrer-Gonzalez, F.X., Fu, H., Nowinski, B., Olofsson, M., Powers, M.A., et al., 2022. The Ocean's labile DOC supply chain. Limnol. Oceanogr. 67 (5), 1007–1021. https://doi.org/10.1002/lno.12053.

Moran, M.A., Kujawinski, E.B., Stubbins, A., Fatland, R., Aluwihare, L.I., Buchan, A., et al., 2016. Deciphering ocean carbon in a changing world. Proc. Natl. Acad. Sci. U. S. A 113 (12), 3143–3151. https://doi.org/10.1073/pnas.1514645113.

Murphy, K.R., Stedmon, C.A., Graeber, D., Bro, R., 2013. Fluorescence spectroscopy and multi-way techniques. PARAFAC. Anal. Methods 5 (23), 6557–6566. https://doi.org/10.1039/c3ay41160e.

Nalven, S.G., Ward, C.P., Payet, J.P., Cory, R.M., Kling, G.W., Sharpton, T.J., et al., 2020. Experimental metatranscriptomics reveals the costs and benefits of dissolved organic matter photo-alteration for freshwater microbes. Environ. Microbiol. 22 (8), 3505–3521. https://doi.org/10.1111/1462-2920.15121.

Nercessian, O., Noyes, E., Kalyuzhnaya, M.G., Lidstrom, M.E., Chistoserdova, L., 2005. Bacterial populations active in metabolism of C1 compounds in the sediment of Lake Washington, a freshwater lake. Appl. Environ. Microbiol. 71 (11), 6885–6899. https://doi.org/10.1128/AEM.71.11.6885-6899.2005.

Neufeld, J.D., Schafer, H., Cox, M.J., Boden, R., McDonald, I.R., Murrell, J.C., 2007. Stable-isotope probing implicates Methylophaga spp and novel Gammaproteobacteria in marine methanol and methylamine metabolism. ISME J. 1 (6), 480–491. https://doi.org/10.1038/ismej.2007.65.

Obernosterer, I., Reitner, B., Herndl, G.J., 1999. Contrasting effects of solar radiation on dissolved organic matter and its bioavailability to marine bacterioplankton. Limnol. Oceanogr. 44 (7), 1645–1654. https://doi.org/10.4319/lo.1999.44.7.1645.

Seidel, M., Yager, P.L., Ward, N.D., Carpenter, E.J., Gomes, H.R., Krusche, A.V., et al., 2015. Molecular-level changes of dissolved organic matter along the Amazon River-to-ocean continuum. Mar. Chem. 177, 218–231. https://doi.org/10.1016/j.marchem.2015.06.019.

Shmareva, M.N., Doronina, N.V., Tarlachkov, S.V., Vasilenko, O.V., Trotsenko, Y.A., 2018. Methylophaga muralis bur 1, a haloalkaliphilic methylotroph isolated from the khilganta soda lake (Southern transbaikalia, buryat republic). Microbiology 87 (1), 33–46. https://doi.org/10.1134/S0026261718010162.

Siegel, D.A., Maritorena, S., Nelson, N.B., Hansell, D.A., Lorenzi-Kayser, M., 2002. Global distribution and dynamics of colored dissolved and detrital organic materials. Journal of Geophysical Research-Oceans 107 (C12). https://doi.org/10.1029/2001jc000965, 21-21-21-14.

Sleighter, R.L., Mckee, G.A., Hatcher, P.G., 2009. Direct Fourier transform mass spectral analysis of natural waters with low dissolved organic matter. Org. Geochem. 40 (1), 119–125. https://doi.org/10.1016/j.orggeochem.2008.09.012.

Song, X., Zhao, Y., Zhang, L., Xie, X., Wu, J., Wei, Z., et al., 2022. Photodegradation, bacterial metabolism, and photosynthesis drive the dissolved organic matter cycle in the Heilongjiang River. Chemosphere 295, 133923. https://doi.org/10.1016/j.chemosphere.2022.133923.

Stubbins, A., Dittmar, T., 2015. Illuminating the deep: molecular signatures of photochemical alteration of dissolved organic matter from North Atlantic Deep Water. Mar. Chem. 177, 318–324. https://doi.org/10.1016/j.marchem.2015.06.020.

Stubbins, A., Spencer, R.G.M., Chen, H.M., Hatcher, P.G., Mopper, K., Hernes, P.J., et al., 2010. Illuminated darkness: molecular signatures of Congo River dissolved organic matter and its photochemical alteration as revealed by ultrahigh precision mass spectrometry. Limnol. Oceanogr. 55 (4), 1467–1477. https://doi.org/10.4319/lo.2010.55.4.1467.

Teeling, H., Fuchs, B.M., Becher, D., Klockow, C., Gardebrecht, A., Bennke, C.M., et al., 2012. Substrate-controlled succession of marine bacterioplankton populations induced by a phytoplankton bloom. Science 336 (6081), 608–611. https://doi.org/10.1126/science.1218344.

Thorn, K.A., Younger, S.J., Cox, L.G., 2010. Order of functionality loss during photodegradation of aquatic humic substances. J. Environ. Qual. 39 (4), 1416–1428. https://doi.org/10.2134/jeq2009.0408.

Wang, Y., Zhang, R., He, Z., Van Nostrand, J.D., Zheng, Q., Zhou, J., et al., 2017. Functional gene diversity and metabolic potential of the microbial community in an estuary-shelf environment. Front. Microbiol. 8, 1153. https://doi.org/10.3389/fmicb.2017.01153.

Ward, C.P., Nalven, S.G., Crump, B.C., Kling, G.W., Cory, R.M., 2017. Photochemical alteration of organic carbon draining permafrost soils shifts microbial metabolic pathways and stimulates respiration. Nat. Commun. 8 (1), 772. https://doi.org/10.1038/s41467-017-00759-2.

Wei, Z., Li, N., Zhang, X., Zheng, L., Mo, S., Korshin, G., et al., 2023. Characterizing photochemical production carboxyl content of dissolved organic matters using absorbance spectroscopy combined with FT-ICR MS. Chemosphere 344, 140352. https://doi.org/10.1016/j.chemosphere.2023.140352.

Wen, S., Lu, Y., Luo, C., An, S., Dai, J., Liu, Z., et al., 2022. Adsorption of humic acids to lake sediments: compositional fractionation, inhibitory effect of phosphate, and implications for lake eutrophication. J. Hazard Mater. 433, 128791. https://doi.org/10.1016/j.jhazmat.2022.128791.

Wetzel, R.G., Hatcher, P.G., Bianchi, T.S., 2003. Natural photolysis by ultraviolet irradiance of recalcitrant dissolved organic matter to simple substrates for rapidbacterial metabolism. Limnol. Oceanogr. 40 (8), 1369–1380. https://doi.org/10.4319/lo.1995.40.8.1369.

Williams, R.J., Howe, A., Hofmockel, K.S., 2014. Demonstrating microbial co-occurrence pattern analyses within and between ecosystems. Front. Microbiol. 5, 358. https://doi.org/10.3389/fmicb.2014.00358.

Yin, G.G., Zhang, P., Wang, Y.H., Aftab, B., Du, P.H., Zhang, Q., et al., 2023. Photochemical transformation of terrestrial dissolved organic matter derived from multiple sources in tropical plantations. Geochem. Cosmochim. Acta 358, 162–173. https://doi.org/10.1016/j.gca.2023.08.016.

Zhang, Z., Chen, Y., Wang, R., Cai, R., Fu, Y., Jiao, N., 2015. The fate of marine bacterial exopolysaccharide in natural marine microbial communities. PLoS One 10 (11), e0142690. https://doi.org/10.1371/journal.pone.0142690.

Zheng, Q., Chen, Q., Cai, R., He, C., Guo, W., Wang, Y., et al., 2019. Molecular characteristics of microbially mediated transformations of Synechococcus-derived dissolved organic matter as revealed by incubation experiments. Environ. Microbiol. 21 (7), 2533–2543. https://doi.org/10.1111/1462-2920.14646.

Zheng, Q., Wang, Y., Xie, R., Lang, A.S., Liu, Y., Lu, J., et al., 2018. Dynamics of heterotrophic bacterial assemblages within synechococcus cultures. Appl. Environ. Microbiol. 84 (3). https://doi.org/10.1128/AEM.01517-17.